ORIGINAL PAPER

Synthesis, Structure, Luminescent and Intramolecular Proton Transfer in Some Imidazole Derivatives

Jayaraman Jayabharathi · Venugopal Thanikachalam · Natesan Srinivasan · Kanagarathinam Saravanan

Abstract A group of novel 2-aryl imidazole derivatives were synthesized and characterized by NMR spectra, X-ray, mass and CHN analysis. An excited state intramolecular proton transfer (ESIPT) process in hydroxy imidazoles (dmip and dmtip) have been studied using emission spectroscopy and it was detected that the two distinct ground state rotamers of I and II are responsible for the normal and the tautomer emission respectively. In hydrocarbon solvent, the tautomer emission predominates over the normal emission for both dmip and dmtip. This reveal that rotamer II is responsible for the tautomer emission and it is stabler than rotamer I which causes the normal emission. In alcoholic solvent like ethanol, a dramatic enhancement of normal emission is observed which was due to increased solvation, the more polar rotamer I become stabler than rotamer II. In dioxane—water mixtures it is observed that the addition of water inhibits the ESIPT process due to the formation of the intermolecular hydrogen bonding involving water. DFT calculations on energy, dipole moment, charge distribution of the rotamers in the ground and excited states of the imidazole derivatives were performed and discussed. PES calculation indicates that the energy barrier for the interconversion of two rotamers is too high in the excited state than the ground state.

Keywords NMR · X-ray · ESIPT · PES · CIS

J. Jayabharathi (✉) · V. Thanikachalam · N. Srinivasan · K. Saravanan
Department of Chemistry, Annamalai University,
Annamalainagar 608 002 Tamilnadu, India
e-mail: jtchalam2005@yahoo.co.in

Introduction

Excited state intramolecular proton transfer (ESIPT) phenomena have been investigated [1–13] in the past decades due to the practical applications of ESIPT exhibiting molecules as laser dyes [1], photostabilizers [11], fluorescent probes in biology [13] and light-emitting materials for electroluminescent devices [6, 7]. ESIPT typically occurs in aromatic molecules having a phenolic hydroxy group with an intramolecular hydrogen bond to the nearby hetero atom of the same chromophore. The proton in the hydroxy group upon photoexcitation migrates to the hetero atom at a distance <2Å to form the excited state tautomer. The two distinct intramolecular hydrogen bonded rotamers I and II (Fig. 1) have been detected experimentally in the ground state [3] by the typical ESIPT exhibiting 2-(2′-hydroxyphenyl)benzazole derivatives. It is established that only rotamer II undergoes ESIPT to form the excited state phototautomer III, which transmits a long wavelength emission with a large Stokes shift of 200 nm, while rotamer I is responsible for the short wavelength normal emission. It is therefore possible for the ESIPT exhibiting substances to have dual fluorescence, depending on the molecular nature and the external factors such as solvent polarity and temperature.

The ESIPT process involves very fast transfer of the hydroxyl (or amino) proton to an acceptor such as carbonyl oxygen or nitrogen atom in an excited state of a molecule, resulting in the formation of the keto tautomer (III) from the initial enol tautomer (II) [14, 15]. Then the excited keto tautomerluminesce, undergoing a transition to the ground state, the reverse proton transfer takes place and the molecule returns to the enol form. The ESIPT process usually manifested in steady state spectra in an significantly large Stokes shift of the fluorescence spectrum relative to
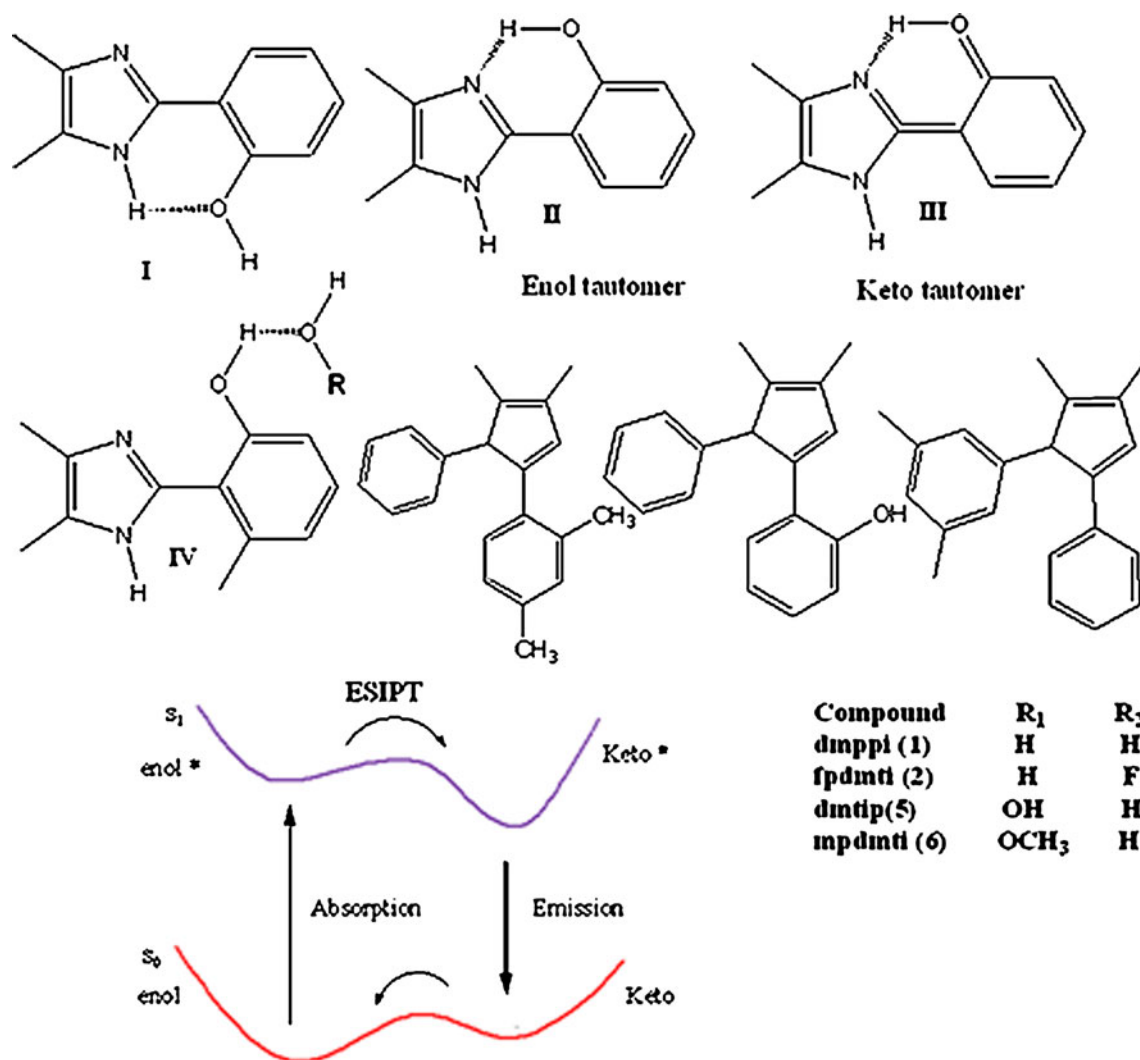
Fig. 1 Various rotameric forms of dmip (**4**) and dmtip (**5**)

the initial absorption spectrum [16–22]. In the present paper, we will focus the light on the photophysical studies of 2-aryl imidazole derivatives (**1–6**), ESIPT process of hydroxy imidazoles (dmip (**4**) and dmtip (**5**)) by comparing their photophysical properties and Density Functional Theory (DFT) calculations on energy and dipole moment of various species, NLO property, HOMO-LUMO energies and PES studies of the two rotamers I and II were performed and discussed.

Experimental

Materials and Methods

Butane-2,3-dione (Sigma-Aldrich Ltd.), *p*-tolualdehyde (S.D. fine.), salicylaldehyde, *o*-anisaldehyde and all other reagents used without further purification.

Optical Measurements and Composition Analysis

NMR spectra were recorded for the 2-aryl imidazole derivatives (**1–6**) on a Bruker 400 MHz. The ultraviolet–visible (UV–Vis) spectra were measured on UV–Vis spectrophotometer (Perkin Elmer, Lambda 35) and corrected for background due to solvent absorption. Photoluminescence (PL) spectra were recorded on a (Perkin Elmer LS55) fluorescence spectrometer. MS spectra were recorded on a Varian Saturn 2200 GCMS spectrometer.

Non-Linear Optical Measurements

Its second harmonic generation efficiency was assessed by Kurtz powder technique [23] at IISc., Bangalore, India. It is a well established tool to evaluate the conversion efficiency of nonlinear optical materials. A Q-switched Nd:YAG laser operating at the fundamental wavelength of 1,064 nm,

generating about 4.1 mJ and pulse width of 8 ns was used for the present experimental study. The input laser beam was passed through an IR reflector and then incident on the powder form of the specimen, which was packed in a glass capillary tube. The output energy was detected by a photodiode detector integrated with oscilloscope assembly.

Computational Details

Quantum mechanical calculations were used to carry out the optimized geometry, NLO, PES, HOMO-LUMO energies and excited state parameters by CIS method with Guassian-03 program using the Becke3-Lee-Yang-Parr (B3LYP) functional supplemented with the standard 6–31G(d,p) basis set [24]. As the first step of our DFT calculation, the geometry taken from the starting structure was optimized and for NLO analysis, the electric dipole moment μ and β tensor components of the imidazole derivatives (1–6) were calculated.

The β_{tot} (total first hyperpolarisability) for the 2-aryl imidazole derivatives (1–6) and the components of the first hyperpolarisability can be calculated using the following equation,

$$\beta_i = \beta_{iii} + 1/3 \sum_{i \neq j} (\beta_{ijj} + \beta_{jij} + \beta_{jji}) \tag{1}$$

Using the x, y and z components, the magnitude of the first hyperpolarisability tensor can be calculated by,

$$\beta_{tot} = (\beta_x^2 + \beta_y^2 + \beta_z^2)^{1/2} \tag{2}$$

The complete equation for calculating the magnitude of first hyperpolarisability from Gaussian-03 output is given as follows,

$$\beta_{tot} = [(\beta_{xxx} + \beta_{xyy} + \beta_{xzz})^2 + (\beta_{yyy} + \beta_{yzz} + \beta_{yxx})^2 \tag{3}$$
$$+ (\beta_{zzz} + \beta_{zxx} + \beta_{zyy})^2]^{1/2}$$

$$\alpha = (\alpha_{xx} + \alpha_{yy} + \alpha_{zz}) 1/3 \tag{4}$$

All the electric dipole moment and the first hyperpolarisability were calculated by taking the Cartesian coordinate system $(x, y, z)=(0, 0, 0)$ at own center of mass of the compounds (1–6).

General Procedure for the Synthesis of 2-aryl Imidazole Derivatives (1–6)

The experimental procedure was used as the same as described in our recent papers [25, 26]. The 2-aryl imidazole derivatives (1–6) were synthesized from an unusual four components assembling of Butane-2,3-dione, ammonium acetate, substituted anilines and substituted benzaldehydes.
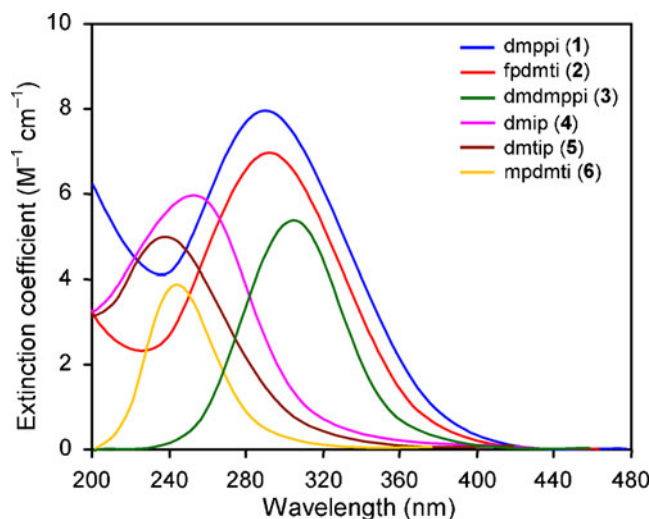

Fig. 2 Excitation spectra of 2-aryl imidazole derivatives **1–6**

4,5-Dimethyl-1-(p-tolyl)-2-phenyl-1H-imidazole (dmppi), (1)

Yield: 40%. mp 125 °C, Anal. calcd. for $C_{18}H_8N_2$: C, 82.41; H, 6.92; N, 10.68. Found: C, 82.02; H, 6.69; N, 10.70. ^{1}H NMR (400 MHz, CDCl$_3$): δ 2.42 (s, 3H), 2.31 (s, 3H), 2.02 (s, 3H), 7.02–7.36 (aromatic protons). ^{13}C (100 MHz, CDCl$_3$): δ 9.57, 12.76, 21.19, 125.45, 127.54, 127.63, 127.97, 128.01, 130.11, 130.92, 133.41, 135.34, 138.37, 145.15. MS: m/z 262.00, calcd. 262.35.

2-(4-fluorophenyl)-4,5-dimethyl-1-p-tolyl-1H-imidazole (fpdmti) (2)

Yield: 40%. mp 130 °C, Anal. calcd. for $C_{18}H_{17}FN_2$: C, 77.12; H, 6.11; N, 9.99. Found: C, 77.00; H, 5.98; N, 9.03. ^{1}H NMR (400 MHz, CDCl$_3$): δ 2.01 (s, 3H), 2.29 (s, 3H), 2.43 (s, 3H), 6.87–7.34 (aromatic protons). ^{13}C (100 MHz,
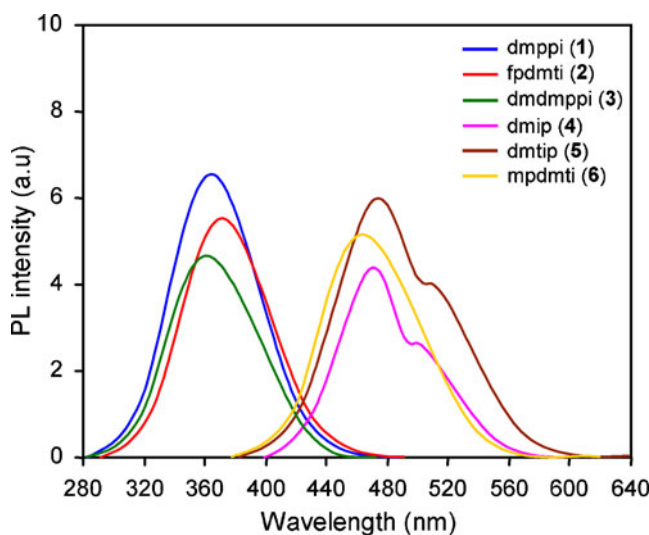

Fig. 3 Emission spectra of 2-aryl imidazole derivatives **1–6**

Table 1 Photophysical spectral parameters of 2-arylimidazole derivatives (1–6) in dioxane

Compound	λ_{abs} (nm)	λ_{exi} (nm)	λ_{flu} (nm)	ΔE cm^{-1}
dmppi (1)	290.5 (303.9)	290.0 (303.0)	362.0 (359.7)	6799 (5104.6)
fpdmti (2)	291.5 (280.0)	292.0 (282.0)	365 (360.4)	6908 (7967)
dmdmppi (3)	303.9 (274.1)	304.0 (272.0)	360.0 (360.0)	5128 (8705)
dmip (4)	248.0 (231.0)	248.5 (231.0)	470.0, 500.0 (sh) (453.0)	19046 (21215)
dmtip (5)	238.5 (227.0)	239.0 (226.5)	478.0, 510.0 (sh) (422.0)	21008.2 (20356.0)
mpdmti (6)	245.0 (298.5)	244.5 (290.0)	460.0 (452.0)	19077 (11377)

Values in the parenthesis are recorded in ethanol

CDCl$_3$): δ 9.53, 12.69, 21.18, 114.92, 115.10, 125.44, 127.16, 129.89, 130.20, 133.35, 135.13, 138.57, 144.28, 161.26, 163.23. MS: m/z 280.00, calcd. 280.14.

4,5-dimethyl-1-(3,5-dimethylphenyl)-2-phenyl-1H-imidazole (dmdmppi) (3)

Yield: 40%. mp 142 °C, Anal. calcd. for C$_{19}$H$_{20}$N$_2$: C, 82.57; H, 7.29; N, 10.14. Found: C, 82.00; H, 6.89; N, 9.72. ^{1}H NMR (400 MHz, CDCl$_3$): δ 1.98 (s, 3H), 2.27 (s, 3H), 2.29 (s, 6H), 6.77–7.36 (aromatic protons). ^{13}C (100 MHz, CDCl$_3$): δ 9.65, 12.77, 21.27, 125.54, 125.59, 127.59, 127.97, 128.03, 130.02, 130.07, 133. 53, 137.88, 139.33, 144.98. MS: m/z 276.00, calcd. 276.16.

2-(4,5-dimethyl-1H-imidazol-2-yl)phenol (dmip) (4)

Yield: 45%. mp 115 °C, Anal. calcd. for C$_{11}$H$_{12}$N$_2$O: C, 70.19; H, 6.43; N, 14.88. Found: C, 70.00; H, 5.89; N, 14.00. ^{1}H NMR (400 MHz, CDCl$_3$): δ 2.27 (s, 3H), 2.30 (s, 3H), 6.79–7.31, (aromatic protons), 10.30 (s, 1H). ^{13}C (100 MHz, CDCl$_3$): δ 9.53, 12.26, 116.40, 121.00, 127.23, 130.53, 146.08, 154.30. MS: m/z 188.00, calcd. 188.09.

2-(4,5-dimethyl-1-p-tolyl-1H-imidazol-2-yl)phenol (dmtip) (5)

Yield: 42%. mp 150 °C, Anal. calcd. for C$_{18}$H$_{18}$N$_2$O: C, 77.67; H, 6.52; N, 10.06. Found: C, 77.00; H, 5.89; N, 9.82. ^{1}H NMR (400 MHz, CDCl$_3$): δ 2.20 (s, 3H), 2.31 (s, 3H),2.40 (s, 3H), 6.88–7.30 (aromatic protons), 11.62 (s, 1H). ^{13}C (100 MHz, CDCl$_3$): δ 9.53, 12.69, 21.18, 116.20, 118.00, 121.00, 127.23, 130.00, 134.48, 137.90, 144.31, 155.28. MS: m/z 278.00, calcd. 278.14.

2-(2-methoxyphenyl)-4,5-dimethyl-1-p-tolyl-1H-imidazole (mpdmti) (6)

Yield: 42%. mp 169 °C, Anal. calcd. for C$_{19}$H$_{20}$N$_2$O: C, 78.05; H, 6.89; N, 9.58. Found: C, 78.00; H, 6.29; N, 9.82. ^{1}H NMR (400 MHz, CDCl$_3$): δ 2.20 (s, 3H), 2.31 (s, 3H), 2.45 (s, 3H), 3.95 (s, 3H), 6.83–7.37 (aromatic protons). ^{13}C (100 MHz, CDCl$_3$): δ 9.45, 11.70, 24.51, 55.82, 114.8,

115.6, 121.56, 122.32, 123.62, 129.80, 130.08, 135.29, 145.82. MS: m/z 292.00, calcd. 292.16.

Results and Discussion

All 2-aryl imidazole derivatives (1–6) fluoresces strongly in solutions at room temperature. Their luminescence excitation spectra (Fig. 2) are in coincide with their absorption spectra and differ from their emission spectra (Fig. 3). Therefore, the fluorescence of the 2-aryl imidazole derivatives (1–6) was taken for discussion. Fluorescence band maximum (λ_{flu}) fluorescence excitation maximum (λ_{exc}) and Stokes shifts (ΔE) are presented in Table 1 for 1–6.

It maybe suggested that in aprotic solvents, the hydroxy substituted 2-aryl imidazoles namely dmip (4) and dmtip (5) exists as two different intramolecular hydrogen bonded isomers I and II (Fig. 4). Excitation of the isomer II should lead to the formation of the keto-isomer III due to ESIPT (Fig. 1), while excitation of the isomer I must yield the normal emission. But, we found out that the fluorescence spectra of dmip (4) and dmtip (5) in dioxane contain an abnormal Stokes-shifted emission band and one small shoulder peak at higher wavelength which reveal that only the isomer II of these molecules is stable under these conditions. Stokes shift is important for a fluorescent
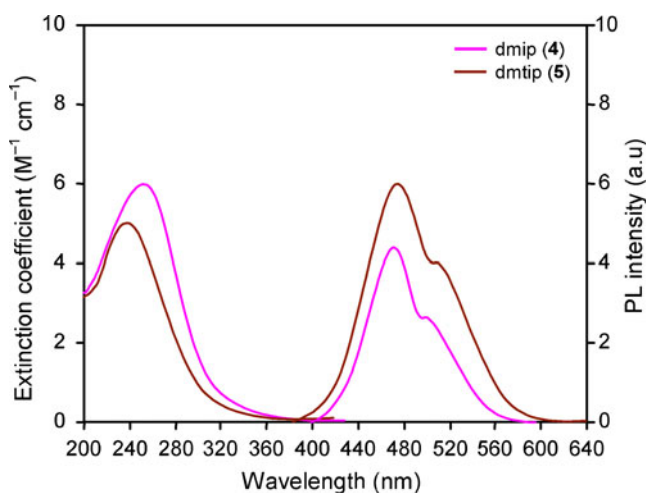

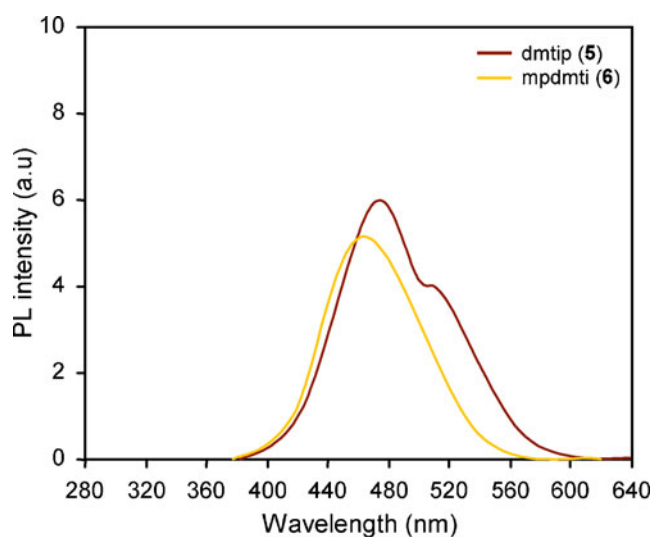**Fig. 4** Excitation and emission spectra of dmip (4) and dmtip (5)

Table 2 Electron density of atoms N(5) and O for dmip (**4**) and dmtip (**5**)

Compound	Atom	II	II*	III
dmip (**4**)	N(5)	−0.390	−0.432	0.312
	O	−0.571	−0.523	−0.692
dmtip (**5**)	N(5)	−0.330	−0.402	0.304
	O	−0.458	−0.435	−0.526

*Excited state enol isomer

sensor. The higher stokes shift value supplies very low background signals and resultantly allows the usage of the material in construction of a fluorescence sensor [27]. However, in the case of hydroxyl containing solvent (EtOH), a short wavelength emission band appears for dmip (**4**) and dmtip (**5**) which is absent in the fluorescence spectra of **1**–**3** and **6** (Fig. 4). This result corresponds to the data obtained earlier [26, 28] for compounds demonstrating ESIPT and can be explained by the presence of intermolecular hydrogen bonding with solvent molecule leading to the stabilization of solvated isomer IV in which ESIPT is impossible.

For better understanding the ESIPT mechanism in dmip (**4**) and dmtip(**5**), we performed DFT calculation of electron density for the keto and enol isomers of the dmip (**4**) and dmtip(**5**) molecules in the ground and the excited states (Table 2) which reveal that excitation of enol isomer leads to an increase in the electron density at the N (5) atom and decrease at the O atom resulting in ESIPT and formation of the excited keto isomer in excited state. Then the excited keto isomer emits luminescence and returns to the ground state keto form, which is characterized by a large positive charge at the N (5) atom and negative charge at the O atom.

As a result, a reverse process occurs in the ground state of the molecule producing an initial molecule in the enol form.

Correlation Between Intramolecular Hydrogen Bonding and ESIPT Process

The existence of intramolecular hydrogen bond in hydroxy substituted imidazoles namely dmip (**4**) and dmtip (**5**) is confirmed by the presence of the singlet at 10.30 ppm (dmip) and 11.62 ppm (dmtip) in the 1H NMR spectra which is a typical signal for hydrogen bonded hydrogen atom. In order to reveal the contribution of the intramolecular hydrogen bonding in the hydroxy imidazoles dmip (**4**) and dmtip (**5**) to their optical properties, the fluorescence spectra of compounds dmdip (**5**) and its derivative mpdmti (**6**) were measured in dioxane solvent under identical condition (Fig. 5). A dual fluorescence was detected for dmtip (**5**) with emission peak centered at 478 and 510 nm respectively. The emission peak at shorter wavelength at 478 nm is assigned to rotamer I and longer wavelength band at 510 nm is assigned to rotamer II [3] whereas compound mpdmti (**6**) exhibits emission peak only at 460 nm, absence of additional peak at longer wavelength confirms that absence of intramolecular hydrogen bond in compound mpdmti (**6**) which further evident that intramolecular hydrogen bond is the essential driving force for ESIPT and the dual fluorescence behaviour of dmtip (**5**).

Competition of Intra and Intermolecular Hydrogen Bonding in Binary Solvents

The competition of intra and intermolecular hydrogen bonding in dmip (**4**) and dmtip (**5**) derivatives were studied in dioxane-water. In this binary-solvent solution, dioxane is
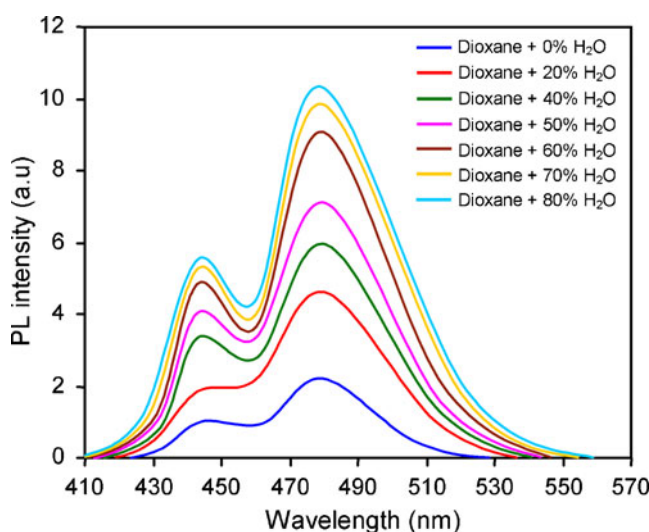
Fig. 5 Fluorescence spectra of dmtip (**5**) and mpdmti (**6**)

Fig. 6 Fluorescence spectra of dmtip (**5**) in dioxane-water mixed solvents

Table 3 Relative energies[a] (eV) and dipole moments (D) in the ground and excited state for rotamers I, II and III

Compound	Rotamers	Ground state		Excited state	
		μ (D)	E(eV)	E(eV)	μ(D)
dmip (4)	I	3.62	0.04 (0.00)	3.89 (3.42)	8.25
	II	3.23	0.08 (0.03)	4.12 (3.76)	8.02
	III	5.49	0.58 (0.32)	3.52 (3.14)	4.56
dmtip (5)	I	4.03	0.01 (0.00)	4.23 (4.02)	7.84
	II	3.62	0.04 (0.02)	3.92 (3.46)	8.52
	III	5.28	0.42 (0.28)	3.56 (3.04)	3.45

[a] Relative energies are calculated with respect to the ground state minimum energy form in ethanol. Values in the parenthesis are recorded in ethanol

a non polar and weakly hydrogen bonding solvent in which normal emission is weak while water is a protic but poor solvent for most of the organic molecules. For this purpose, a series of solutions in dioxane-water mixture with different water fraction but identical concentrations of dmtip (**5**) were made for spectroscopic measurements. As shown by the normalized fluorescence spectra (Fig. 3), dmtip(**5**) exhibits both normal and tautomer emission peaks at 478 and 510 nm respectively in pure dioxane. With the addition of water, the tautomer emission intensity decreases relatively to that of the normal emission. When water fraction is increased to 20% (v/v), the tautomer emission almost vanished. With further increasing water fraction to 40% (v/v), a new emission band at 445 nm appeared in addition to the normal emission. This band intensity increased with increasing water fraction and turned to be the main emission when water fraction is high up to 80% (v/v) (Fig. 6). It is understandable that the tautomer emission decreases with increasing water fraction in the mixed solvent if the intermolecular hydrogen bonding between dmtip (**5**) and water is taken into account. In the initial stage, the presence of small amount of water in the dioxane solution must give rise to solvation of dmtip (**5**). The intermolecular hydrogen bonding between dmtip (**5**) and water definitely disrupts the ground state intramolecular hydrogen bonding rotamers I and II but increases the quantity of species IV, in which ESIPT and tautomer formation are inhibited. Consequently the tautomer emission decreases with addition of water and finally vanished.

Density Functional Theory Calculation

The ESIPT phenomenon has inspired a large number of theoretical calculations [28–30]. The ground-state geometries of the three species, I, II, and III for both dmip (**4**) and dmtip(**5**) were optimized using the DFT/6-31G (d,p) method. Complete optimization of all the geometrical parameters gives the ground state energy of each species. The energy of the excited state was calculated using the standard CIS method. Table 3 gives the energies and dipole
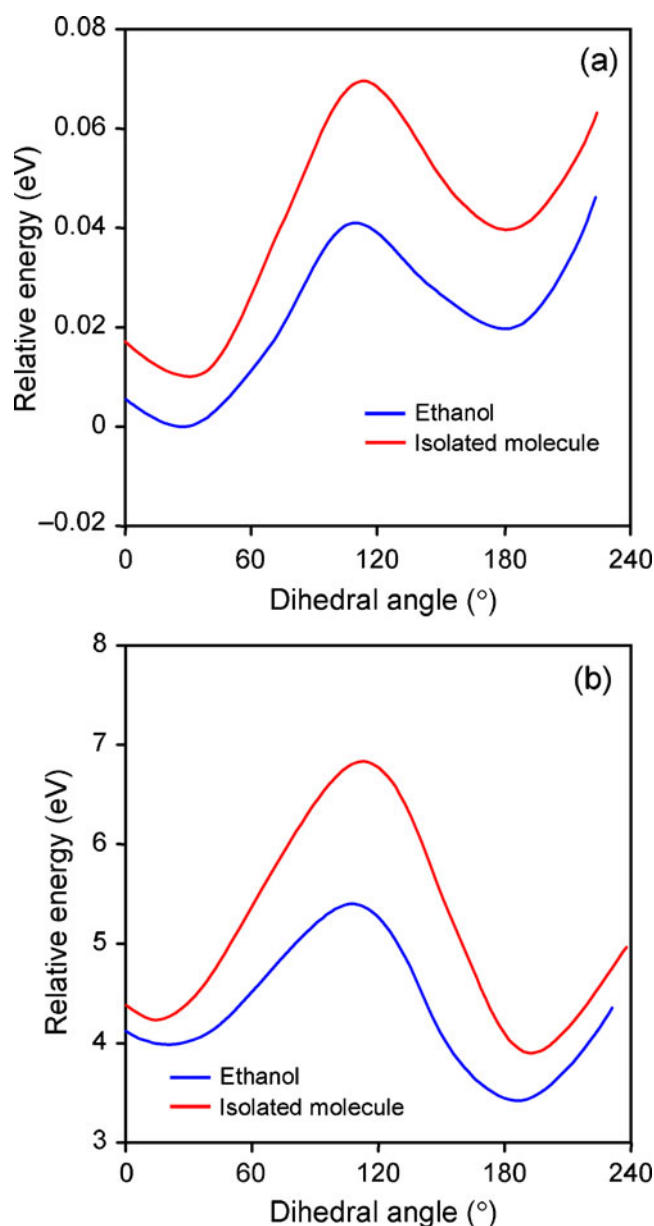

Fig. 7 **a**. PES for the interconversion of the rotamers of dmip (**4**) in the ground state. **b**. PES for the interconversion of the rotamers of dmip (**4**) in the excited state

Table 4 Quantum yield and thermodynamic parameters of imidazole derivatives **1**–**6**

Compound	ϕ_f	τ_f (ns)	k_r (ns^{-1})	k_{nr} (ns^{-1})	HOMO (a.u)	LUMO (a.u)	Eg (a.u)
dmppi (1)	0.71	1.42	0.50	0.20	−0.1984	−0.0168	0.1816
fpdmti (2)	0.44	1.44	0.30	0.39	−0.2794	−0.1157	0.1637
dmdmppi (3)	0.60	1.61	0.37	0.25	−0.2059	−0.0441	0.1619
dmip (4)	0.42	1.72	0.24	0.34	−0.1997	−0.0297	0.1770
dmtip (5)	0.49	1.35	0.30	0.44	−0.1894	−0.0183	−0.1711
mpdmti (6)	0.51	1.31	0.40	0.36	−0.2648	−0.099	0.1658

moment of the species I, II, and III in the ground and the excited state. For better understanding the ESIPT mechanism in dmip (**4**) and dmtip(**5**), we performed DFT calculation of electron density for the keto and enol isomers of the dmip (**4**) and dmtip(**5**) in the ground and the excited states (Table 2).

In the excited state the nitrogen atom becomes richer in electrons than the hydroxylic oxygen atom. This redistribution of the π-electron densities in the excited electronic state is the driving force for the intramolecular proton transfer from the hydroxylic group to the nitrogen atom. The potential energy (PE) curves (Fig. 7a and b) for the interconversion of isomers I and II of dmtip (**5**) in the

ground and the excited states reveal that for isolated dmtip (**5**) in the ground state the barrier for interconversion is 4.5 kcal/mol and 3.4 kcal/mol in ethanol. In the excited state the barrier for dmtip (**5**) in the isolated molecule and in the alcohol medium are 12.5 and 9.8 kcal/mol, respectively. The barriers for interconversion in the excited state is much higher than that in the ground state (Table 3).

Quantum Yield and Thermodynamic Parameters of 2-aryl Imidazole Derivatives (**1-6**)

The fluorescence quantum yield for compounds **1**–**6** (Table 4) were measured in acetonitrile using coumarin 47
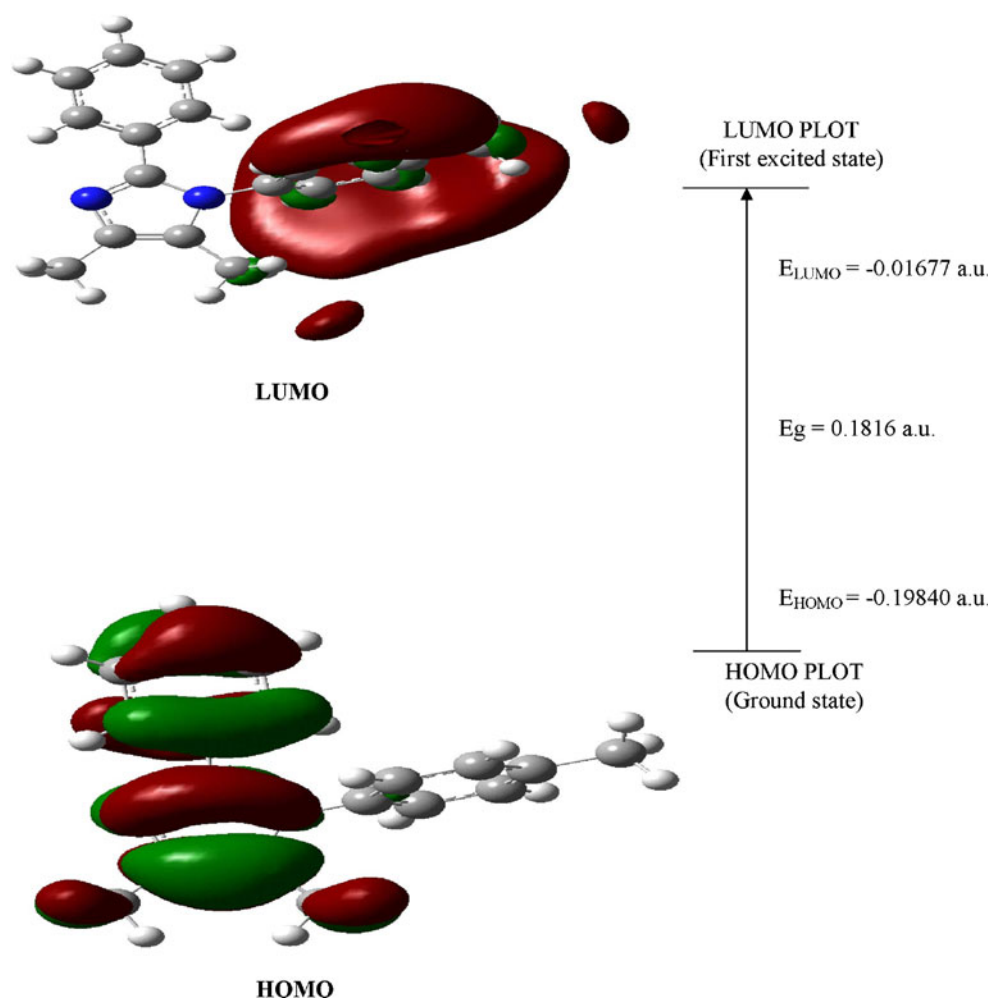

Fig. 8 HOMO-LUMO orbital picture of dmppi (1)

LUMO

LUMO PLOT
(First excited state)

$E_{LUMO} = -0.01677$ a.u.

Eg = 0.1816 a.u.

$E_{HOMO} = -0.19840$ a.u.

HOMO PLOT
(Ground state)

HOMO

Table 5 Electric dipole moment (D), polarizability (α) and hyperpolarizability (β_{total}) of (1–6)

Parameter	dmppi (1)	fpdmti (2)	dmdmppi (3)	dmip (4)	dmtip (5)	mpdmti (6)
Electric dipole moment (D)						
μ_x	4.1575	−1.6667	−2.8610	−0.4584	−0.4015	−0.0538
μ_y	−0.2181	−3.6836	−1.0621	0.8072	−0.8858	0.4505
μ_z	0.2560	−1.4874	−1.1603	−1.2426	1.0729	0.4463
μ_{total}	4.1711	4.3081	3.2649	1.5510	−0.2144	0.8430
Polarizability (α)						
α_{xx}	168.02	323.342	311.922	321.177	180.5289	229.4428
α_{xy}	−0.760	−3.123	4.169	−1.469	34.0782	37.9341
α_{yy}	0.002	264.943	250.777	286.834	133.8131	99.4140
α_{xz}	0.062	12.572	0.188	−8.127	−39.1104	−43.7296
α_{yz}	119.264	5.881	26.507	0.767	−34.5488	−8.5868
α_{zz}	43.391	103.467	114.336	96.133	614.3149	640.1431
$\alpha \times 10^{-24}$ (esu)	70.47	34.1725	33.4455	34.7847	45.876	47.869
Hyperpolarizability (β_{total})						
β_{xxx}	889.0866	433.7337	105.6872	43.1135	33.5059	−68.8788
β_{xxy}	1.1910	−125.9418	−94.7286	−46.0440	−28.5833	−29.6330
β_{xyy}	2.2085	−69.0532	−67.0422	110.5338	−14.8611	−3.992
β_{yyy}	11.1018	−273.7393	43.4894	149.2485	−93.1900	53.4965
β_{xxz}	143.6161	−175.4702	−51.1599	−21.7770	−29.4058	37.1521
β_{xyz}	−11.4331	75.9236	37.0878	133.0105	45.4424	60.8972
β_{yyz}	−26.3634	46.0494	20.9672	43.1935	172.1898	63.8108
β_{xzz}	−20.0420	43.0301	86.448	119.2973	539.3020	478.3876
β_{yzz}	−23.8558	−69.0634	−23.6013	10.2854	202.4031	21.3076
β_{zzz}	−199.3893	−30.1211	−9.3178	−52.7186	−7631.1062	−8608.0030
$\beta \times 10^{-31}$ (esu)	75.6105	55.4131	43.4238	45.6805	64.836	73.590

as a standard according to the equation,

$$\Phi_{unk} = \Phi_{std} \left(\frac{I_{unk}}{I_{std}} \right) \left(\frac{A_{std}}{A_{unk}} \right) \left(\frac{\eta_{unk}}{\eta_{std}} \right)^2 \qquad (5)$$

Where Φ_{unk}, Φ_{std}, I_{unk}, I_{std}, A_{unk}, Φ_{unk} and Φ_{std} are the fluorescence quantum yields, the integration of the emission intensities, the absorbances at the excitation wavelength and the refractive indexes of the corresponding solution of the 2-aryl imidazole derivatives (1–6) and the standard, respectively.

The main decay route of the excited state of these compounds (1–6) and their radiative and non-radiative decay are studied in detail. The radiative (k_r) and non-radiative (k_{nr}) rate constants are calculated using the following equations

$$k_r = \Phi_p / \tau \qquad (6)$$

$$k_{nr} = 1/\tau - \Phi_p / \tau \qquad (7)$$

$$\tau = (k_r + k_{nr})^{-1} \qquad (8)$$

Where k_r, k_{nr} are the radiative and non-radiative deactivation, τ_f is the life time of the S_1 excited state. From the view point of the decay rate constants, two trends are evident for the imidazole derivatives 1−6. From the Table 4 it was suggested that the radiative rate constant (k_r) increases when the imidazoles (1,3 and 5) are substituted by electron releasing substituents like methyl and methoxy whereas in the case of fluoro substituted imidazole (2) the radiative rate constant (k_r) decreases.

HOMO-LUMO Energies of Imidazole Derivatives 1–6 by DFT Method

The Eigen values of HOMO, LUMO and their energy gap reflect the chemical activity of the molecule and recently the energy gap between highest occupied molecular orbital (HOMO) and the lowest unoccupied molecular orbital (LUMO) have been used to prove the bioactivity from intramolecular charge transfer (ICT) [31–33]. The HOMO-LUMO energy gap for 1–6 were calculated by B3LYP/6-31G(d,p) and from the HOMO-LUMO orbital picture (Fig. 8) of dmppi (1), it was found that the filled π orbital (HOMO) is mostly located on the phenyl ring attached to

the carbon of the imidazole derivative and the unfilled π* orbital (LUMO) located on the imidazole ring with the phenyl ring attached to the nitrogen of the imidazole ring. Therefore, introduction of an electron-donating substituent into the phenyl ring attached to the nitrogen raises the energy of the LUMO resulting in a blue-shift of the emission. On the otherhand, the introduction of the electron-donating substituent into the aldehydic phenyl ring raises the energy of the HOMO, leading to the red shift of the emission [34, 35]. The calculated energy gap explains the eventual charge transfer interactions within the molecule.

Second Harmonic Generation (SHG) Studies of 2-aryl Imidazole Derivatives (1–6)

Second harmonic signal of 75 mV, 12 mV, 16 mV, 23 mV, 25 mV and 17 mV were obtained for imidazole derivatives **1–6** by an input energy of 4.1 mJ/pulse. But the standard KDP crystal gave a SHG signal of 110 mV/pulse for the same input energy. The second order nonlinear efficiency will vary with the particle size of the powder sample [36] and higher efficiencies are achieved by optimizing the phase matching [37]. On a molecular scale, the extent of charge transfer (CT) across the NLO chromophore determines the level of SHG output, the greater the CT, the larger is the SHG output.
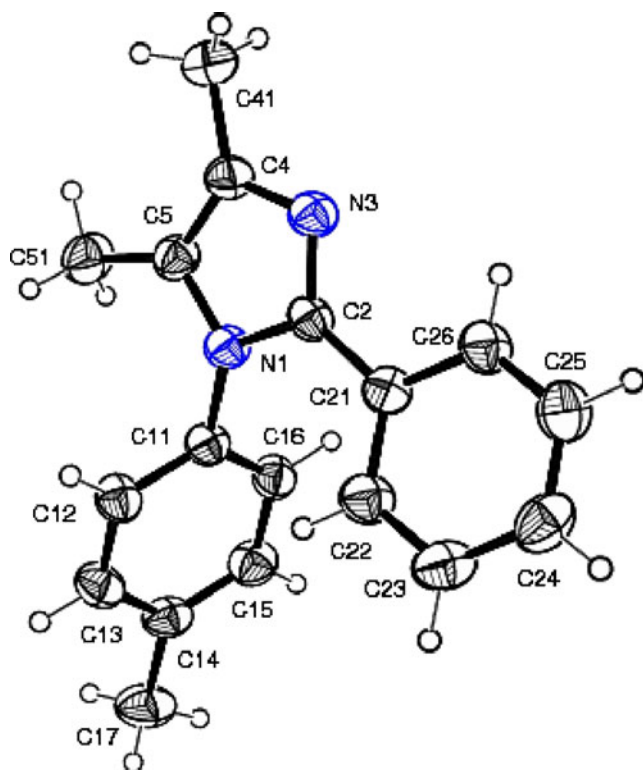
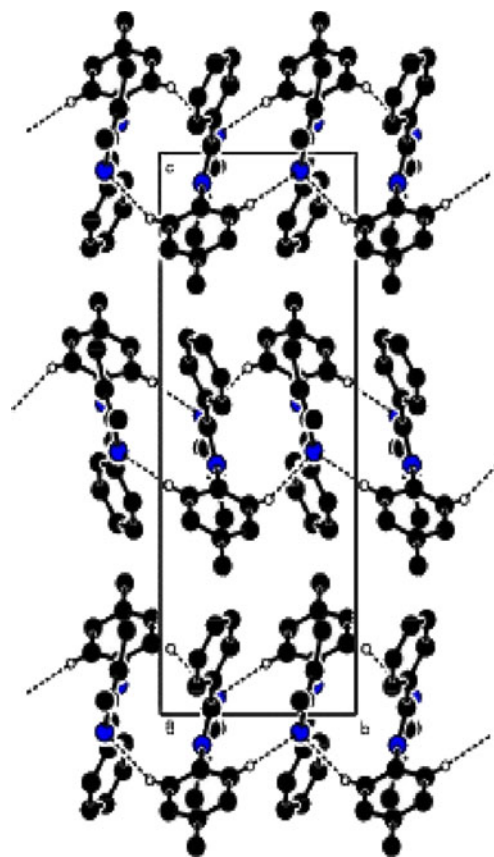**Fig. 9** ORTEP diagram of dmppi (1)

Fig. 10 The packing of the title compound, viewed down the axis. *Dashed lines* indicate hydrogen bonds. H atoms not involved in hydrogen bonding have been omitted

Hyperpolarizability of Imidazole Derivatives 1–6 by DFT Method

In addition to well known empirical rules to estimate qualitatively the microscopic nonlinear response in imidazole derivatives **1–6**, DFT calculation is a more accurate prediction of the NLO activity [38, 39]. The value of second order optical susceptibility in a given NLO system depends on the molecular hyperpolarizability (β), the number of chromophores and the degree of noncentrosymmetry. From Table 5, it was suggested that these compounds **1–6** are polar having non-zero dipole moment, hyperpolarizabilities and hence have well microscopic NLO behaviour [40–42]. To determine the transference region and hence to know the suitability of these compounds **1–6** for microscopic nonlinear optical applications, the UV-visible spectra have been recorded by using the spectrometer in the range of 190–1,100 nm. These compounds show absorption spectra in the UV region between 210 and 290 nm. The increased transparency in the visible region might enable the microscopic NLO behaviour with non-zero values [27, 43, 44]. All the absorption bands are due to π→π* transitions. The β values (Table 5) computed here might be correlated with

Table 6 Selected Bond lengths (Å), Bond angles (°) and torsional angles (°) of dmppi (**1**)

Bond connectivity	Experimental XRD (Å)	Bond angles	Experimental XRD (°)	Torsional angles	Experimental XRD(°)
N1-C2	1.372(1.380)	C2-N1-C5	107.2(107.0)	C5-N1-C2-N3	−0.4(−0.1)
N1-C5	1.388(1.407)	C2-N1-C11	128.6(128.1)	C5-N1-C2-C21	−176.6(−179.6)
N1-C11	1.443(1.429)	C5-N1-C11	123.0(124.5)	C11-N1-C2-N3	−167.5(−173.4)
N3-C2	1.322(1.306)	C2-N3-C4	106.4(107.6)	C11-N1-C2-C21	16.3(6.2)
N3-C4	1.373(1.395)	N1-C2-N3	110.4(110.1)	C2-N1-C5-C4	−0.1(−0.1)
C2–C21	1.467(1.474)	N1-C2-C21	126.7(126.4)	C2-N1-C5-C51	−178.7(−179.1)
C4-C5	1.359(1.354)	N3-C2-C21	122.8(123.4)	C11-N1-C5-C4	167.9(173.9)
C4-C41	1.498(1.495)	N3-C4-C5	110.4(109.4)	C11-N1-C5-C51	−10.7(−5.5)
C5-C51	1.485(1.496)	N3-C4-C41	121.3(120.0)	C2-N1-C11-C12	−119.5(−111.6)
C11-C12	1.382(1.384)	C5-C4-C41	128.3(130.6)	C2-N1-C11-C16	63.6(68.7)
C11-C16	1.380(1.385)	N1-C5-C4	105.6(105.9)	C5-N1-C11-C12	75.3(75.0)
C12-C13	1.386(1.387)	N1-C5-C51	123.0(122.0)	C5-N1-C11-C16	−101.6(−103.7)
C13-C14	1.387(1.390)	C4-C5-C51	131.4(132.1)	C4-N3-C2-N1	0.7(0.2)
C14-C15	1.385(1.391)	N1-C11-C12	119.9(120.1)	C4-N3-C2-C21	177.1(179.8)
C14-C17	1.511(1.516)	N1-C11-C16	119.2(119.9)	C2-N3-C4-C5	−0.8(−0.3)
C15-C16	1.385(1.385)	C12-C11-C16	120.8(120.0)	C2-N3-C4-C41	177.3(179.4)
C21-C22	1.390(1.392)	C11-C12-C13	119.2(119.8)	N1-C2-C21-C22	18.9(26.3)
C21-C262	1.385(1.394)	C12-C13-C14	121.2(120.9)	N1-C2-C21-C26	−164.6(−156.1)
C22-C23	1.383(1.387)	C13-C14-C15	118.1(118.5)	N3-C2-C21-C22	−156.9(−154.1)
C23-C24	1.380(1.385)	C13-C14-C17	120.3(120.9)	N3-C2-C21-C26	19.6(23.4)
C24-C25	1.372(1.388)	C15-C14-C17	121.6(120.6)	N3-C4-C5-N1	0.5(0.2)
C25-C26	1.373(1.383)	C14-C15-C16	121.6(121.0)	N3-C4-C5-C51	179.0(179.0)
C12-H12	0.930(1.073)	C11-C16-C15	119.0(119.8)	C41-C4-C5-N1	−177.3(−179.4)
C13-H13	0.930(1.074)	C2-C21-C22	123.8(123.5)	C41-C4-C5-C51	1.1(1.3)
C15-H15	0.930(1.074)	C2-C21-C26	118.1(117.5)	N1-C11-C12-C13	−176.4(−179.9)
C16-H16	0.930(1.073)	C22-C21-C26	118.1(119.0)	C16-C11-C12-C13	0.4(0.2)
C17-H17A	0.960(1.086)	C21-C22-C23	120.7(120.3)	N1-C11-C16-C15	177.6(179.8)
C17-H17B	0.960(1.083)	C22-C23-C24	120.1(120.4)	C12-C11-C16-C15	0.7(0.4)
C17-H17C	0.960(1.084)	C23-C24-C25	119.4(119.5)	C11-C12-C13-C14	−0.9(−0.1)
C22-H22	0.930(1.069)	C24-C25-C26	120.6(120.3)	C12-C13-C14-C15	0.3(0.1)
C23-H23	0.930(1.073)	C21-C26-C25	121.4(120.5)	C12-C13-C14-C17	179.5(179.3)
C24-H24	0.930(1.073)	C11-C12-H12	120.0(119.7)	C13-C14-C15-C16	0.9(0.1)
				C17-C14-C15-C16	−178.3(−179.0)
				C14-C15-C16-C11	−1.4(−0.4)
				C2-C21-C22-C23	176.8(178.2)

UV-visible spectroscopic data in order to understand the molecular-structure and NLO relationship in view of a future optimization of the microscopic NLO properties. Therefore, the validity of B3LYP/6-31G (d, p) approximation used in all the computations here might also be illustrated by analyzing the relationship between calculated β values and measured values of λ_{max} (Table 1). The band at around 285 nm exhibits a solvatochromic shift, characteristic of a large dipole moment (Table 5) and frequently suggestive of a large hyperpolarizability (Tables 5). These compounds show red shift in absorption with increasing solvent polarity, accompanied with the upward shifts non-zero values in the β-components [20].

X-Ray Analysis

Crystal Structure

Crystalline imidazole derivatives dmppi (**1**) and fpdpi (**2**) [45] are monoclinic crystals. dmppi (**1**) (Fig. 9) crystallizes in the space group p$_n$ and cell has dimensions of a=9.809 Å, b=7.700 Å, c=19.907 Å. ORTEP diagram of dmppi (**1**)

(Fig. 9) shows that the imidazole ring is essentially planar. The imidazole ring makes dihedral angles of 70.91 (19°) and 19.8 (2°) with the *p*-tolyl ring (C11-C16) attached to the nitrogen of the imidazole nucleus and phenyl ring (C21-C26) attached to the carbon of the imidazole nucleus respectively. The dihedral angle between the two phenyl rings is 74.59 (18°). The crystal packing is stabilized by C12-H12···N3 (2-x, 2-y, -z) and C16-H16···N3 (2-x, 1-y, -z) intermolecular hydrogen bonds (Fig. 10). From XRD data, the shortening of bond angles C2-N1-C5, C2-N3-C4 and N1-C5-C4 and increase of bond angles C2-N1-C11, C5-N1-C11, N1-C2-C21, N3-C2-C21, C5-C4-C41and C2-C21-C22 from 120° exactly at the substitution of the imidazole nucleus. This asymmetry of dihedral angles and bond angles reveal the conjugation of the phenyl ring attached to the carbon with the imidazole nucleus. Optimization of dmppi (**1**) have been performed by DFT at B3LYP/6-31 G(d,p) using Gaussian-03 (Table 6). All these XRD data are in good agreement with the theoretical values (Table 6). However, from the theoretical values it can be found that most of the optimized bond lengths, bond angles and dihedral angles are slightly higher than that of XRD values. These deviations can be attributed to the fact that the theoretical calculations were aimed at the isolated molecule in the gaseous phase and the XRD results were aimed at the molecule in the solid state.

Conclusion

Intermolecular hydrogen bonding of dmip (**4**) and dmtip(**5**) with water giving rise to IV impede the ESIPT process, resulting in an increase in the quantum yield of normal emission at the expense of the tautomer emission. However, the intermolecular hydrogen bonding with alcohol is not strong enough to compete with the intramolecular hydrogen bonding in hydroxy substituted imidazole derivatives. Hence, tautomer emission dominates over normal emission in alcohol at room temperature. The DFT calculations indicate that excitation of rotamer II molecule leads to increase in the electron density at the N (5) atom and decrease at O atom resulting in ESIPT and formation of the excited keto isomer III in excited state. Then, the excited keto isomer III emits luminescence and returns to the ground state keto form III, which is characterized by large positive charge at the N (5) atom and negative charge at the O atom. As a result, a reverse process occurs in the ground state of the molecule, producing an initial molecule in the form enol. In the excited state, the nitrogen atom becomes richer in electrons than the hydroxylic oxygen atom. This redistribution of the π-electron densities in the excited electronic state is the driving force for the intramolecular

proton transfer from the hydroxylic group to the nitrogen atom. PES calculation reveals that the barriers for interconversion in the excited state are much higher than that in the ground state. The solution grown good quality of dmppi single crystal belongs to monoclinic crystal system having the space group of Pₙ. Further work we focused the increased transparency of imidazole derivatives in the visible region might enable the microscopic NLO behavior with non-zero values and all the absorption bands are due to only π-π* transition. The higher value of specific heat shows that these compounds are more resistant to laser damage threshold compared to potassium dihydrogen phosphate. Its phase matching and relative second harmonic generation efficiency was determined by using Nd: YAG laser as a source. Its electric dipole moments, polarizability, hyperpolarisability and HOMO-LUMO energies studies were determined by DFT calculation.

References

1. Chou PT, Martinez ML, Clements JH (1993) Reversal of excitation behavior of proton-transfer vs. charge-transfer by dielectric perturbation of electronic manifolds. J Phys Chem 97:2618–2622
2. Gai F, Rich RL, Petrich JW (1994) Monophotonic ionization of 7-azaindole, indole, and their derivatives and the role of overlapping excited states. J Am Chem Soc 116:735
3. Das K, Sarkar N, Ghosh AK, Majumdar D, Nath DN, Bhattacharyya K (1994) Excited state intramolecular proton transfer in 2-(2′-hydroxyphenyl) benzimidazole and -benzoxazole: effect of rotamerism and hydrogen-bonding. J Phys Chem 98:9126
4. Roberts EL, Dey J, Warner IM (1997) Excited-state intramolecular proton transfer of 2-(2′-hydroxyphenyl)benzimidazole in cyclodextrins and binary solvent mixtures. J Phys Chem A 101:5296–5301
5. Agmon N (2005) Elementary steps in excited-state proton transfer. J Phys Chem A 109:13–35
6. Park S, Kwon OH, Lee YS, Jang DJ, Park SY (2007) Imidazole-based excited-state intramolecular proton-transfer (ESIPT) materials: observation of thermally activated delayed fluorescence (TDF). J Phys Chem A 111:9649–9653
7. Park S, Seo J, Kim SH, Park SY (2008) Tetraphenylimidazole-based excited-state intramolecular proton-transfer molecules for highly efficient blue electroluminescence. Adv Funct Mater 18:726–731
8. Qian Y, Li S, Zhang G, Wang Q, Wang S, Xu H, Li C, Li Y, Yang G (2007) Aggregation-induced emission enhancement of 2-(2′-Hydroxyphenyl)benzothiazole-based excited-state intramolecular proton-transfer compounds. J Phys Chem A 111:5861–5868
9. LeGourriérec D, Kharlanov VA, Brown RG, Rettig W (2000) Excited-state intramolecular proton transfer (ESIPT) in 2-(2′-

hydroxyphenyl)-oxazole and –thiazole. J Photochem Photobiol, A Chem 130:101–111

10. Rodembusch FS, Campo LF, Stefani V, Rigacci A (2005) The first silica aerogels fluorescent by excited state intramolecular proton transfer mechanism (ESIPT). J Mater Chem 15:1537–1541

11. Campo LF, Rodembusch FS, Stefani V (2006) New fluorescent monomers and polymers displaying an intramolecular proton-transfer mechanism in the electronically excited state (ESIPT). IV. Synthesis of acryloylamide and diallylamino benzazole dyes and its copolymerization with MMA. J Appl Polym Sci 99:2109–2116

12. Rodembusch FS, Leusin FP, Campo LF, Stefani V (2007) Excited state intramolecular proton transfer in amino 2-(2′-hydroxyphenyl) benzazole derivatives: effects of the solvent and the amino group position. J Lumin 126:728–734

13. Wu Y, Peng X, Fan J, Gao S, Tian M, Zhao J, Sun S (2007) Fluorescence sensing of anions based on inhibition of excited-state intramolecular proton transfer. J Org Chem 72:62–66

14. De Prasad S, Ash S, Dalai S, Mishra A (2007) A DFT-based comparative study on the excited states intramolecular proton transfer in 1-hydroxy-2-naphthaldehyde and 2-hydroxy-3-naphthaldehyde. J Mol Struc, Theochem 807:33–41

15. Gostev FE, Kol'tsova LS, Petrukin AN, Titov AA, Shiyonok AI, Zaichenko NL, Marevtsev VS, Sarkisov OM (2003) Spectral luminescent properties and dynamics of intramolecular processes in 2, 4, 5-triarylimidazoles. J Photochem Photobiol, A Chem 156:15–22

16. Sastre R, Costela A (1995) Polymeric solid-state dye lasers. Adv Mater 7:198–207

17. Chou P, McMorrow D, Aartsma TJ, Kasha M (1984) The proton-transfer laser. Gain spectrum and amplification of spontaneous emission of 3-hydroxyflavone. J Phys Chem 88:4596–4599

18. Stueber GJ, Kieninger M, Schetter H, Busch W, Goeller B, Franke J, Kramer HEA, Hoier H, Henkel S, Fischer P, Port H, Hirsch T, Rytz G, Birbaum JL (1995) Ultraviolet Stabilizers of the 2-(2′-Hydroxyphenyl)-1, 3, 5-triazine class: structural and spectroscopic characterization. J Phys Chem 99:10097–10109

19. Catalan J, Fabero F, Guijarro MS, Clarumunt RM, Santa Maria MD (1999) Photoinduced intramolecular proton transfer as the mechanism of ultraviolet stabilizers: a reappraisal. J Am Chem Soc 112:747–759

20. Volmer F, Rettig W (1996) Fluorescence loss mechanism due to large-amplitude motions in derivatives of 2, 2′-bipyridyl exhibiting excited-state intramolecular proton transfer and perspectives of luminescence solar concentrators. J Photochem Photobiol, A Chem 95:143–155

21. Charles Potter AS, Brown RG (1988) Excited-state intramolecular proton transfer in polar solutions of 2-(2′-hydroxyphenyl) benzothiazole. Chem Phy Lett 153:7–12

22. Jaworski A, Degórski A (1995) A theoretical study of the photoinduced intramolecular proton transfer in 2-(2′-hydroxyphenyl)-imidazoline. Comput Chem 19:189–197

23. Flom SR, Barbara PF (1983) The photodynamics of 2-(2′-hydroxy-5′-methylphenyl)-benzotriazole in low-temperature organic glasses. Chem Phy Lett 94:488–493

24. Guassian 03 program, (Gaussian Inc., Wallingford CT) (2004)

25. Jayabharathi J, Thanikachalam V, Saravanan K (2009) Effect of substituents on the photoluminescence performance of Ir(III) complexes: synthesis, electrochemistry and photophysical properties. J Photochem Photobiol A Chem 208:13–20

26. Saravanan K, Srinivasan N, Thanikachalam V, Jayabharathi J (2010) Synthesis and photophysics of some novel imidazole derivatives used as sensitive fluorescent chemisensors. J Fluoresc. doi:10.1007/s10895-010-0690-5

27. Ismet Kaya MY (2010) Synthesis of a novel fluorescent schiff base as a possible Cu(II) Ion selective sensor. J Fluoresc. doi:10.1007/s10895-010-0620-6

28. Barbara PF, Walsh PK, Brus LE (1989) Picosecond kinetic and vibrationally resolved spectroscopic studies of intramolecular excited-state hydrogen atom transfer. J Phys Chem 93:29–34

29. Woolfe GJ, Melzig M, Schneider S, Dörr F (1983) The role of tautomeric and rotameric species in the photophysics of 2-(2′-hydroxyphenyl) benzoxazole. Chem Phys 77:213–221

30. Sobolewski AL (1993) On the mechanism of excited-state hydrogen transfer in 2-hydroxypyridine. Chem Phys Lett 211:293

31. Fukui K, Yonezawa T, Shingu H (1952) A molecular orbital theory of reactivity in aromatic hydrocarbons. J Chem Phys 20:722–725

32. Padmaja L, Ravikumar C, Sajan D, Hubert Joe I, Jayakumar VS, Pettit GR, Neilsen OF (2009) Density functional study on the structural conformations and intramolecular charge transfer from the vibrational spectra of the anticancer drug combretastatin-A2. J Raman Spectrosc 40:419–428

33. Ravikumar C, Hubert Joe I, Jayakumar VS (2008) Charge transfer interactions and nonlinear optical properties of push-pull chromophore benzaldehyde phenylhydrazone: A vibrational approach. Chem Phys Lett 460:552–558

34. Sun Q, Li Z, Zeng X, Ge M, Wang D (2005) Structures and properties of the hydrogen-bond complexes: Theoretical studies for the coupling modes of the pyrazole-imidazole system. J Mol Struct Theochem 724:167–172

35. Chai SY, Zhou R, An ZW, Kimura A, Fukuho K, Matsumura M (2005) 5-Coordinated aluminium complexes having two 2,4-dimethyl-8-hydroxyquinoline ligands and a phenolic ligand as possible materials for white emission organic light emitting devices. Thin Solid Films 479:282–287

36. Porter Y, OK KM, Bhuvanesh NSP, Halasyamani PS (2001) Synthesis and characterization of Te_2SeO_7: a powder second-harmonic-generating study of TeO_2, Te_2SeO_7, Te_2O_5, and $TeSeO_4$. Chem Mater 13:1910–1915

37. Narayana Bhat M, Dharmaprakash SM (2002) Growth of nonlinear optical γ-glycine crystals. J Cryst Growth 236:376–380

38. Karakas A, Elmali A, Unver H, Svoboda I (2004) Nonlinear optical properties of some derivatives of salicylaldimine-based ligands. J Mol Struct 702:103–110

39. Unver H, Karakas A, Elmali A (2004) Nonlinear optical properties, spectroscopic studies and structure of 2-hydroxy-3-methoxy-N-(2-chloro-benzyl)-benzaldehyde-imine. J Mol Struct 702:49–54

40. Lee IS, Shin DM, Yoon Y, Shin SM, Chung YK (2003) Synthesis and non-linear optical properties of (alkyne)dicobalt octacarbonyl complexes and their substitution derivatives. Inorg Chim Acta 343:41–50

41. Mang C, Wu K, Zhang M, Hong T, Wei Y (2004) First-principle study on second-order optical nonlinearity of some ferrocenyl complexes. J Mol Struct Theochem 674:77–82

42. Justin Thomas KR, Lin JT, Wen YS (1999) Synthesis, spectroscopy and structure of new push-pull ferrrocene complexes containing heteroaromatic rings (thiophene and furan) in the conjugation chain. J Organomet Chem 575:301–309

43. Prabhu SG, Rao PM, Bhat SI, Upadyaya V, Inamdar SR (2001) Growth and characterization of N-(2-Chlorophenyl)-(1-Propanamide)-a nonlinear organic crystal. J Cryst Growth 233:375–379

44. Crasta V, Ravindrachary V, Bharantri RF, Gonsalves R (2004) Growth and characterization of an organic NLO crystal: 1-(4-methylphenyl)-3-(4-methoxyphenyl)-2-propen-1-one. J Cryst Growth 267:129–133

45. Gayathri P, Jayabharathi J, Srinivasan N, Thiruvalluvar A, Butcherc RJ (2010) 2-(4-Fluorophenyl)-4, 5-dimethyl-1-(4-methylphenyl)-1H-imidazole. Acta Crystallogr E66:o1703